Journal of Aerosol Science 64 (2013) 103–110

Contents lists available at SciVerse ScienceDirect

Journal of Aerosol Science

journal homepage: www.elsevier.com/locate/jaerosci

Particle size distribution of welding fume and its dependency on conditions of shielded metal arc welding

A.A. Ennan, S.A. Kiro, M.V. Oprya, V.I. Vishnyakov *

Physical-Chemical Institute for Environmental and Human Protection, National Academy of Sciences of Ukraine, 3 Preobrazhenskaya, Odessa 65082, Ukraine

ARTICLE INFO

Article history:
Received 23 December 2012
Received in revised form
19 June 2013
Accepted 19 June 2013
Available online 28 June 2013

Keywords:
Shielded metal arc welding
Welding fume
Particle size distribution
Multi-modal distribution
Laser spectrometer

ABSTRACT

The particle size distribution of the shielded metal arc welding fumes is studied. The laser aerosol spectrometer and optoelectronic aerosol counter with the total measurement range of 0.15–10 μm were used. It is demonstrated that the number-based size distribution is described by the three-modal lognormal distribution, where the first two modes are the result of the liquid-phase and solid-phase coagulation and the third mode is the coarse fume particles. The linear dependency of the average size of the particles on the product of welding parameters: the arc resistance, the wire feed rate and the electrode sectional area is revealed.

© 2013 Elsevier Ltd. All rights reserved.

1. Introduction

The processes of arc welding are accompanied by formation of toxic aero-disperse particles in the size range of 0.005–20 μm, representing the danger for human health and environment, which are commonly referred to as 'welding fume'. It is well known that the size and the shape of a particle is a predictor of the site of deposition in the respiratory tract (International Commission on Radiological Protection (ICRP), 1994; Hinds, 1999). In addition, the biological activity of the welding fume inhalable particles, like other slightly soluble substances, depends on their number density, size, shape and specific surface, i.e. is appropriately represented by the lower moments of the particle size distribution (PSD) (Hewett, 1995; Oberdorster et al., 2005). Therefore, the studies allowing to analyze the relationship between the welding fume PSD and the arc welding parameters are of large applied importance.

The welding fume particles are formed by the following processes: nucleation of the vapors of welding materials outside the high-temperature arc discharge zone and growth of the nuclei (the primary particles); coagulation of the primary particles (the agglomerates with different spatial structures and sizes over 0.1 μm); ejection and explosion of the liquid droplets of the electrode-material from the arc or the molten weld pool (coarse fume particles with sizes over 1 μm) (Berlinger et al., 2011; Jenkins et al., 2005; Sowards et al., 2008a; Voitkevich, 1995; Worobiec et al., 2007; Zimmer & Biswas, 2001). When the shielded metal arc welding (SMAW) is applied, the agglomerates of primary particles and coarse fume particles mostly prevail in the welder's breathing-zone. Therefore, while measurements of agglomerate and coarse PSD are determinants of the site of respiratory deposition and biological activity, measuring the chemical composition throughout

* Corresponding author. Tel.: +38 0487237528; fax: +38 0487231116.
E-mail addresses: drvishnyakov@mail.ru, eksvar@ukr.net (V.I. Vishnyakov).

0021-8502/$ - see front matter © 2013 Elsevier Ltd. All rights reserved.
http://dx.doi.org/10.1016/j.jaerosci.2013.06.006

the primary particle size distribution could be informative in understanding the resulting toxicity (Oberdorster, 1996; Richman et al., 2011). The size distribution of agglomerates and their spatial structure can essentially depend on the primary particles' electrical charge formed in the nucleation and growth processes (Onischuk et al., 2000).

The nucleation and growth of the nuclei occurs simultaneously with coagulation. If the colliding primary particles are in the liquid state, their association produces a spherical particle. If the collision happens between solid particles, they form agglomerates. It is difficult to define the agglomerates' real sizes experimentally, because their shape and spatial structure are very complex. Therefore, the existing methods of the welding fume PSD study are based on the measurement of the equivalent diameter instead of the real size (for example, aerodynamic, optical, electrical mobility), i.e. the diameter of the sphere that has the same value of a particular physical property as the real agglomerate.

For example, some authors (Berlinger et al., 2011; Breskey et al., 2012; Sowards et al., 2008b) measured the size distribution of the welding fume generated by SMAW in the size range of 0.05–10 μm with cascade impactors. The measured mass-based PSD obeys the bimodal lognormal distribution with parameters: $d_1 = 0.29$ μm, $\sigma_1 = 1.5$ and $d_2 = 2.6$ μm, $\sigma_2 = 3.29$ (Breskey et al., 2012). Sowards et al. (2008b) approximated the number-based PSD by an unimodal lognormal distribution with the geometric mean diameter $d = 0.1$–0.25 μm and the standard deviation $\sigma = 1.15$–1.25, while the mass-based PSD showed $d = 0.55$–0.75 μm and $\sigma = 1.11$–1.32, depending on the type of electrode coating and welding conditions. They noted also the tendency towards the increase of the geometric mean diameter as the welding heat input increases.

The essential disadvantage of the aerodynamic separation is the destruction of agglomerates when they pass through the impactor cascades and the collection of some coarse fume on the walls, but not on the impaction plates (Reist, 1984). In the present paper, a laser aerosol spectrometer was used for real-time monitoring of the inhalable particles' dispersion. The main aim of the study was to explore the dependence of PSD on the SMAW conditions.

2. Experimental technique and measurement procedure

The mild steel plates were used as a base material for the single-pass surface welding with a direct current of reverse polarity and the electrode travel angle of 45°. The SMAW commercial electrodes covered with rutile (TiO_2) Paton ANO-4 electrodes (American Welding Society (AWS) classification E6012) and the carbonate-fluorite ($CaCO_3$–CaF_2) Paton UONI 13/55 electrodes (AWS classification E6015) were used. The average welding parameters are presented in Table 1.

The welding fume plume was localized by extracting air at a distance of 40 cm from the welding arc with a flow of 75 l s^{-1} (Oprya et al., 2012) and redirected into the vertical pipe with the diameter of 19 cm and length of 120 cm. The air flow rate at the sampling spot was of 270 ± 20 cm s^{-1} (Fig. 1). A specially designed nozzle (2) for isokinetic sampling of the welding fume was used. The welding fume dispersion was measured using the laser aerosol spectrometer LAS-P (LAS-P, 2010). The LAS-P aerosol spectrometer allows determination of the size distribution of particles ranging from 0.15 to 1.5 μm in the media characterized by particle concentrations up to 2×10^3 cm^{-3}. The maximum relative errors in determining the volume of the air samples and the size of particles and their number density is $\pm 5\%$ and $\pm 10\%$ respectively. The multichannel size distribution had the following size ranges (μm): 0.15–0.2, 0.2–0.25, 0.25–0.3, 0.3–0.4, 0.4–0.5, 0.5–0.7, 0.7–1.0, 1.0–1.5, >1.5. The standard optoelectronic aerosol counter OEAC-05 (with channels (μm): 0.5–0.7, 0.7–1.0, 1.0–1.5, 1.5–2, 2–3, 3–5, 5–7, 7–10, >10) was used in parallel.

The particle number density in the sample has the typical value of 10^5–10^6 cm^{-3} which is much more than needed for measurements using LAS-P number density ($\leq 2 \times 10^3$ cm^{-3}). Therefore, the dual-stage dilution system was used (Fig. 1). The first stage (4) has the fixed dilution ratio of 86 at a constant volumetric flow rate of 10 l min^{-1}. The dilution ratio of the second stage (5) depends on the volumetric flow rate of the pre-filtered air (7) and is 5 for the electrodes with the diameter of 3 mm and 4 mm, and 12.5 for the electrodes with the diameter of 5 mm. It provides the total dilution ratio of 430 and

Table 1
Welding parameters.

No.	Electrode type	Electrode diameter D (mm)	Arc voltage U (V)	Welding current I (A)	Wire feed rate v (mm s^{-1})
01	ANO-4	3	28	105	4.1
02	ANO-4	3	33	145	4.8
03	ANO-4	4	29	160	3.8
04	ANO-4	4	34	200	4.5
05	ANO-4	5	29	210	2.9
06	ANO-4	5	34	280	3.5
07	UONI 13/55	3	28	105	3.9
08	UONI 13/55	3	33	140	4.5
09	UONI 13/55	4	28	160	3.5
10	UONI 13/55	4	33	210	4.0
11	UONI 13/55	5	28	215	3.0
12	UONI 13/55	5	33	295	3.5

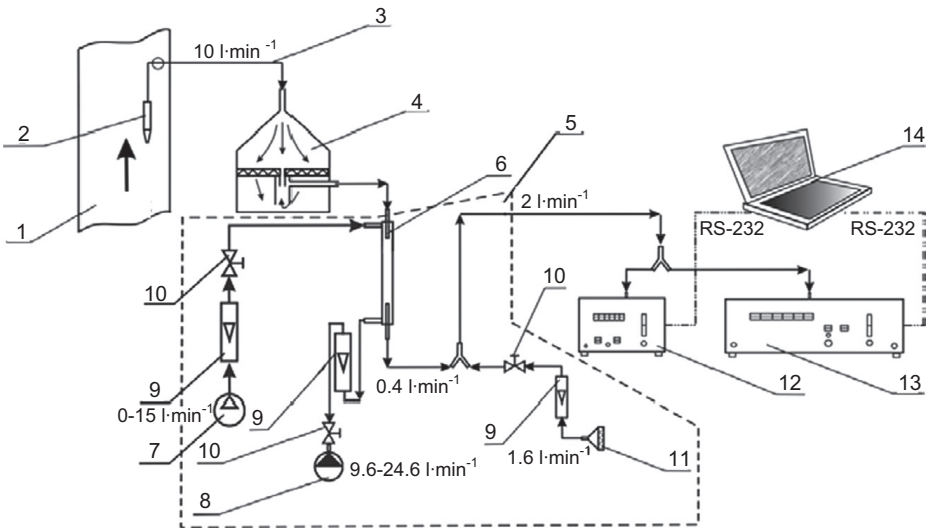

Fig. 1. Scheme of experimental equipment: 1, vertical pipe; 2 and 3, nozzle for isokinetic sampling of the welding fume and the sampling tube respectively; 4, dilution system with the capillary and the bypass flow rate with a fixed dilution ratio (first stage); 5, dilution system with adjustable dilution ratio (second stage); 6, flow divider chamber; 7, compressor; 8, vacuum pump; 9, air flow meters; 10, gas cock; 11, Petryanov's filter; 12, optoelectronic counter OEAC-05; 13, laser aerosol spectrometer LAS-P; 14, computer.

1075 respectively. Petryanov's filters with the collection efficiency of at least 99.97% for the particles with size of 0.15–0.2 μm were used in the dilution system. The distortion of the PSD due to the particles' coagulation in the sampling system or in the dilution system is absent.

3. Experimental results

The fractions of total particle number averaged over ten measurements for each channel of the counters have been obtained. The measurements of the multi-modal number-based PSD can be approximated by linear combination of three weighted lognormal unimodal distributions $f_n(d)$:

$$f(d) = a_1 f_1(d) + a_2 f_2(d) + a_3 f_3(d),$$

where d is the particle diameter; a_i is the distribution coefficient or fraction of the overall PSD;

$$f_i(d) = \frac{1}{d \ln \sigma_i \sqrt{2\pi}} \exp \frac{-(\ln d - \ln d_{0i})^2}{2 \ln^2 \sigma_i},$$

where d_{0i} and σ_i are the geometric mean particle diameter and the standard deviation of the unimodal distribution respectively.

The iterative analysis technique known as the method of nonlinear least squares was used to fit a smooth curve to the observed histograms and to estimate the parameters of the overall PSD. The experimental data and fitted curves for regime No. 6, in which the electrode ANO-4 with the diameter of 5 mm was used, are shown in Fig. 2. The same data are shown in Fig. 3 as the integral distributions by using the probability-logarithmic scale.

As it is seen in the figures, three modes well described the experimental distribution. The measured mean diameters and the parameters of the approximation distributions are presented in Table 2 for all the welding regimes.

The basic mode, whose content in the welding fume is 80–90%, is described by the geometric mean diameter ~0.22 μm. The second mode, whose content is 10–20%, is described by the geometric mean diameter ~0.33 μm. And the third mode, whose content less than 0.2%, represents the coarse fume particles with the sizes over 1 μm.

The measurements demonstrate the absence of correlation between the average particle diameter and the applied heat input $E = UI/v$ (U is the arc voltage; I is the welding current; v is the wire feed rate), as it was proposed by Sowards et al. (2008b). The histograms of the heat input and the experimental values of the mean diameters, incremented ten times for comparability, are presented in Fig. 4.

The search for the welding factor that determines the changes in the number-based PSD (Table 2) has led to the dependencies presented in Fig. 5. The mean diameter of the welding fume particles and the geometric mean diameter of the basic fitted mode linearly depend on the product RvS, where $R = U/I$ is the arc resistance; v is the wire feed rate; $S = \pi D^2/4$ is the electrode wire sectional area.

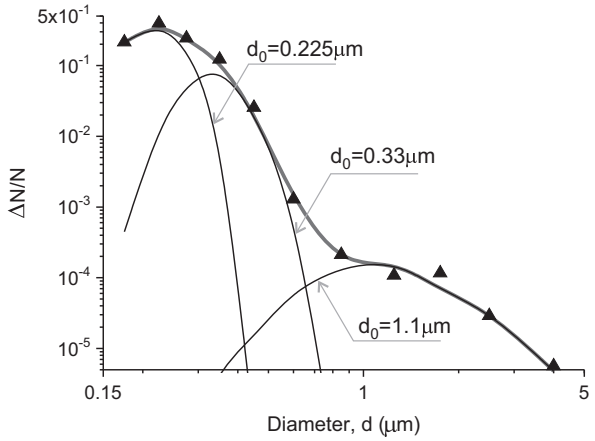

Fig. 2. Number-based PSD for regime No. 6: experimental data (dots) and approximation (resulting is grey curve, fractions are black curves).

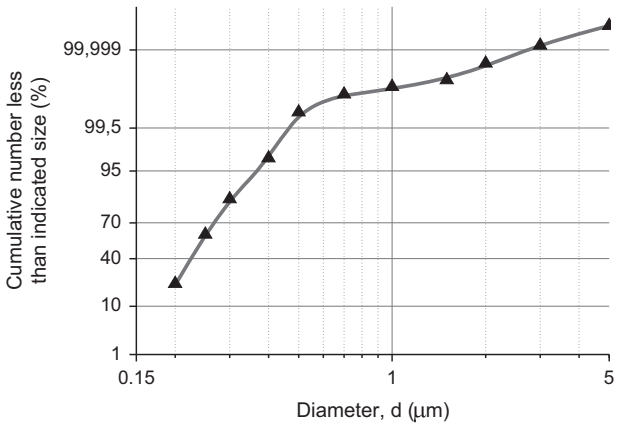

Fig. 3. Integral number-based PSD for regime No. 6: experimental data (dots) and approximation (curve).

Table 2
Mean diameters and parameters of 3-modal approximation (μm).

No.	$\overline{d}$	d_{01}	σ_1	a_1 (%)	d_{02}	σ_2	a_2 (%)	d_{03}	σ_3	a_3 (%)
01	0.241	0.220	1.11	83	0.34	1.15	16.90	1.25	1.4	0.10
02	0.242	0.221	1.11	83	0.35	1.14	16.90	1.20	1.4	0.10
03	0.251	0.226	1.11	80	0.35	1.15	19.90	1.20	1.5	0.10
04	0.262	0.230	1.11	77	0.36	1.14	22.80	1.35	1.4	0.20
05	0.243	0.222	1.11	80	0.33	1.14	19.95	1.15	1.5	0.05
06	0.248	0.225	1.11	78	0.33	1.14	21.95	1.10	1.5	0.05
07	0.221	0.210	1.11	91	0.33	1.13	08.97	1.20	1.4	0.03
08	0.228	0.214	1.11	90	0.33	1.15	09.97	1.70	1.3	0.03
09	0.232	0.218	1.11	86	0.32	1.16	13.97	1.50	1.3	0.03
10	0.240	0.225	1.11	86	0.33	1.16	13.97	1.50	1.4	0.03
11	0.233	0.220	1.11	89	0.33	1.15	10.98	1.20	1.5	0.02
12	0.234	0.221	1.11	88	0.33	1.15	11.98	1.10	1.6	0.02

4. Discussion

4.1. Multi-modal distribution

Some authors describe the number-based PSD of the welding fume as unimodal or bimodal lognormal distribution (Breskey et al., 2012; Sowards et al., 2008b). The study of the measured data demonstrates the existence of the three modes, the first two of which result from the primary particles' coagulation and the third mode is the coarse fume particles.

It is necessary to distinguish two stages of the particles' coagulation. The first stage occurs simultaneously with the nucleation and growth of the primary particles as the coalescence of the droplets, when the temperature is above the condensable matter melting point. The second stage is the coagulation of the solid particles as a result of sporadic collisions.

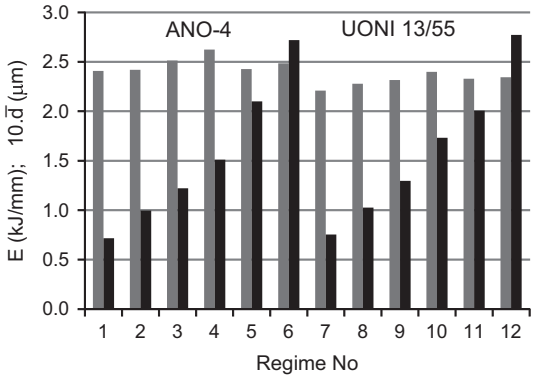

Fig. 4. Histograms of heat input E (black) and ten times incremented mean diameter of particles $\overline{d}$ (grey).

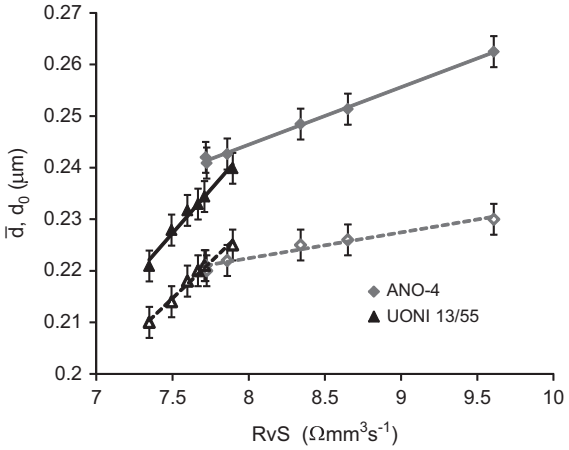

Fig. 5. Dependencies of the measured mean diameter $\overline{d}$ (solid lines) and median of the basic fitted mode d_0 (dashed lines) on the product of the welding parameters.

The large number of the nuclei ($n_n \sim 10^{15}$ cm^{-3}) is the cause of intensive coagulation already at initial moment of nucleation. Evolution of the size distribution function f_n is described by the Smoluchowski equation (Yu et al., 2008):

$$\frac{\partial f_n}{\partial t} = -f_n \int k(n,m) f_m \, dm + \frac{1}{2}\int k(n-m,m) f_{n-m} f_m \, dm, \tag{1}$$

where the association rate of two droplets, consisting of n and m nuclei, is determined by the kernel of the equation

$$k(n,m) = k_0 (n^{1/3} + m^{1/3})^2 \sqrt{\frac{1}{n} + \frac{1}{m}},$$

where $k_0 = \pi r_n^2 \sqrt{8 k_B T / \pi m_n}$; r_n, m_n are the radius and mass of the nucleus respectively.

The evolution of the average number of nuclei contained in the associate droplet is defined by integrating Eq. (1) for the simple distribution function (Smirnov, 2000),

$$\frac{d\overline{n}}{dt} = k_0 n_n I \overline{n}^{1/6}, \tag{2}$$

$$I = \frac{1}{2}\int_0^\infty \int_0^\infty (x^{1/3} + y^{1/3})^2 \sqrt{\frac{1}{x} + \frac{1}{y}} \exp(-x-y)\, dx\, dy = 3.4,$$

which leads to

$$\overline{n} = 3.5 (n_n k_0 t)^{6/5}, \tag{3}$$

accordingly, the average radius of the associate droplets is $r_{cd} = r_n \overline{n}^{1/3}$, and their average number density is $n_{cd} = n_n / \overline{n}$.

When the gas–vapor mixture cools from the initial temperature of the nucleation down to the melting point of condensable matter, with cooling rate ~0.5 K/μs (Tashiro et al., 2010), the coagulation provides the formation of droplets with the average diameter of ~25 nm, and their number density is ~10^{11} cm^{-3}. It is necessary to consider that the nucleation occurs within ~1 ms and all nuclei could be associated with each other and with associate droplets, i.e. all the nuclei and primary particles participate in the coagulation at the nucleation and growth period. Then, as the calculations

show, the average diameter of associate droplets is ~20 nm, and their number density is $\sim 2 \times 10^{11}$ cm^{-3} to the moment when the gas–vapor mixture temperature reaches the iron melting point.

Thus, there are two fractions in the gas–vapor mixture by the moment of phase change. The first fraction consists of the natural primary particles in the form of small droplets with the diameter of ~2 nm and the number density of $\sim 10^{14}$–10^{15} cm^{-3}, which did not have time to associate with each other. The second fraction consists of the relatively large droplets with the diameter of ~20 nm and the number density of $\sim 10^{11}$ cm^{-3}, that transform into uniform spherical solid particles.

Further, the second stage of coagulation begins, that is association of the primary small particles with each other and association of the small particles with the primary large particles (probability of the association of the large particles with each other is negligibly low). In the first case the fluffy structures are formed, including the chain-like and lace-like structures. In the second case the agglomerates represent the structures with the uniform dense core and the friable coating. The formation rate of these structures is defined by the cross section of the small primary particles $\pi r_s^2 \sim 3$ nm^2 and the large primary particles $\pi r_l^2 \sim 300$ nm^2. The calculation with account for these cross sections gives the growth of the agglomerates up to the diameters of $d_s \sim 0.18$ μm and $d_l \sim 0.28$ μm, when the gas–vapor mixture cools down to the temperature of 300 K.

It is clear that these calculations are approximate, because they do not consider that the particle distribution function varies in time. However, even this approximation fairly illustrates the mechanism of forming of the two close modes of agglomerates in the welding fume. Thus, it is possible to suggest that the mode 0.22 μm (Fig. 2) represents the fluffy structures, i.e. results from the small primary particles' agglomeration; and the mode 0.33 μm (Fig. 2) is the structures with the uniform dense core, which are formed as a result of association of the small primary particles and the large primary particles (Berlinger et al., 2011).

4.2. Welding factor determining the size of particles

Let us consider the product $RvS = UvS/I$. The product of the wire feed rate and the electrode sectional area defines the mass consumption of the electrode material:

$$\frac{\Delta m_{El}}{\Delta t} = \rho v S,$$

where ρ is the density of the electrode wire.

About 10% of the electrode material is vaporized during the arc welding. Most of this vapor is condensed in the welding pool, but some part is dispersed and injected into the condensation zone. The carry-over of the vapor from the arc into the condensation zone depends on the arc length, because the size of the cathode spot (reverse polarity) increases, the stability of the arc column decreases and, accordingly, the carry-over of the vapor increases as the arc lengthens (Pires et al., 2006). It is well-known that the arc length is linearly related to the arc voltage $L \sim U$ (Evans et al., 1998). Then, the rate of the carry-over of the vapor from the arc into the condensation zone is

$$\frac{\Delta m_{vap}}{\Delta t} \sim L \frac{\Delta m_{El}}{\Delta t} \sim UvS. \tag{4}$$

Thus, the product UvS defines the substance carry-over rate into the condensation zone. The growth of this parameter leads to increase of the injection of condensable atoms into the zone where nucleation occurs and, accordingly, to increase of the supersaturation of the condensable vapor. As the vapor mixes with air it cools and the supersaturation increases. At some value of supersaturation the nucleation and growth of the nuclei start, and proceed until the melting temperature is reached. The increase of the initial supersaturation leads to earlier beginning of the nucleation and, accordingly, to the increase of the primary particles' growth duration. Thus, the increase of the product UvS leads to the increase of the size of primary particles and the size of agglomerates of these particles, i.e. $\overline{d} \sim UvS$.

The welding current I is determined by the number of the charge carriers, which are electrons in the arc, preferentially. Therefore, the value of the current is directly related to the rate of electron emission from the cathode surface $I = e\, dN_e/dt$. Some part of the emitted electrons diffuses from the cathode region into the condensation zone, enriches the additional electron number density n_e^{arc} with the rate

$$\frac{\Delta n_e^{arc}}{\Delta t} \sim I. \tag{5}$$

The vapor–gas mixture in the condensation zone has the temperature of 2000–3000 K and contains a large number of alkali metal atoms from the electrode coating, which at such temperature are partially ionized and provide the large electron and ion number density. Thus, the condensation occurs in the ionized gas with condensed particles, i.e. in the dusty plasma in which the particles are charged. The charge of the particle of welding fume is defined by the balance of the emission flux from the particle and the electron backflow from the gas to the particle, which increases as the electron number density increases (Vishnyakov, 2012). The particle is charged positively, if the emission flux exceeds the backflow. And it is charged negatively in the opposite case. The backflow depends on the electron diffusion from the cathode. Therefore, increase of n_e^{arc} leads to the decrease of the positive particles' charge and increase of the negative particles' charge.

The particles' charge strongly influences the nucleation process both at the homogenous and heterogeneous ion-induced nucleation as was investigated by Vishnyakov (2008) and Vishnyakov et al. (2013), who have shown that decrease of the

positive particles' charge leads to the shift of the nucleation into the range of lower temperatures. At the same time, the sizes of the nuclei and the primary particles decrease.

Thus, the increase of the welding current at constant vapor formation rate leads to the decrease of the particles' size, because the electron number density in the gas phase is increased, i.e. $\overline{d}\sim I^{-1}$. As a result, from (4) and (5) it follows:

$$\overline{d}\sim\frac{\Delta m_{vap}}{\Delta n_e^{arc}}\sim\frac{UvS}{I}=RvS.$$

This equation describes the tendency of the basic particles' mode (with mean diameter of ~0.2 μm) to change. The average size of the second mode mostly depends on the large primary particles' size, therefore it is feebly subject to the welding regime influence.

5. Conclusion

The presented study demonstrates that the inhalable particles of the welding fume have three-modal particle size distribution, when electrodes with rutile and carbonate-fluorite covers are applied. The consideration of the nucleation, growth of the nuclei and their coagulation showed that the first mode (content of 80–90%), most likely, is represented by the agglomerates of small primary particles which are formed as a result of nucleation and growth of the nuclei in the liquid phase. The second mode (content of 10–20%) is a product of association of the small primary particles with the large primary particles, which are formed as a result of the coagulation of the nuclei in the liquid phase. The third mode (content of 0.02–0.2%) is the coarse fume particles.

The welding fume dispersion does not depend on any single welding parameter, but it depends on the combination of parameters in the form $\overline{d}\sim RvS$. It is defined by the existence of the competitive processes, as the carry-over of the vapors and carry-over of the electrons from the arc region into the condensation zone. The increase of the vapors amount leads to the increase of the particles' average size, and increase of the electron number leads to the average size decrease.

The obtained results could be useful for future welding consumable development and for sanitary-hygienic assessment of welding consumable and operation conditions, since they: (a) add information to inhalation models of welding fume; (b) yield insight into what processes affect the PSD of the welding fumes of the inhalable particles; (c) contribute to development of more rigorous models of the inhalable particle chemistry.

References

Berlinger, B., Benker, N., Weinbruch, S., L'Vov, B., Ebert, M., Koch, W., Ellingsen, D.G., & Thomassen, Y. (2011). Physicochemical characterisation of different welding aerosols. *Analytical and Bioanalytical Chemistry*, *399*(5), 1773–1780.

Breskey, J., Abelmann, A., & Erdal, S. (2012). Particle size distribution of welding fume measured in the breathing-zone and in an emission chamber. In *Proceedings of American Industrial Hygiene Conference and Expo (SR-107-02), Indianapolis, IN, June 2012*. San Francisco: ChemRisk.

Evans, D.M., Huang, D., McClure, j.C., & Nunes, A.C. (1998). Arc efficiency of plasma arc welding. *Welding Journal*, *77*(2), 53-s–58-s.

Hewett, P. (1995). Estimation of regional pulmonary deposition and exposure for fumes from 'SMAW' and 'GMAW' mild and stainless steel consumables. *American Industrial Hygiene Association Journal*, *56*, 136–142.

Hinds, W.C. (1999). *Aerosol Technology* (2nd ed.). Wiley and Sons: New York.

International Commission on Radiological Protection (ICRP) (1994). *Human Respiratory Tract Model for Radiological Protection*, Publication 66. Oxford: Pergamon Press.

Jenkins, N.T., Pierce, W.M.-G., & Eagar, T.W. (2005). Particle size distribution of gas metal and flux cored arc welding fumes. *Welding Journal*, *84*(10), 156-s–163-s.

LAS-P (2010). *Laser Aerosol Spectrometer (LAS-P) model 9814.290.000*. Moscow: Karpov Institute of Physical Chemistry.

Oberdorster, G. (1996). Significance of particle parameters in the evaluation of exposure–dose–response relationships of inhaled particles. *Inhalation Toxicology*, *8*, 73–89.

Oberdorster, G., Maynard, A., Donaldson, K., Castranova, V., Fitzpatrick, J., Ausman, K., Carter, J., Karn, B., Kreyling, W., Lai, D., Olin, S., Monteiro-Riviere, N., Warheit, D., & Yang, H. (2005). Principles for characterizing the potential human health effects from exposure to nanomaterials: elements of a screening strategy. *Particle and Fibre Toxicology*, *2*(8).

Onischuk, A.A., di Stasio, S., Karasev, V.V., Strunin, V.P., Baklanov, A.M., & Panfilov, V.N. (2000). Evidence for long-range coulomb effects during formation of nanoparticle aggregates from pyrolysis and combustion routes. *Journal of Physical Chemistry A*, *104*, 10426–10434.

Oprya, M., Kiro, S., Worobiec, A., Horemans, B., Darchuk, L., Novakovic, V., Ennan, A., & Van Grieken, R. (2012). Size distribution and chemical properties of welding fumes of inhalable particles. *Journal of Aerosol Science*, *45*, 50–57.

Pires, I., Quintino, L., Miranda, R.M., & Gomes, J.F.P. (2006). Fume emissions during gas metal arc welding. *Toxicological and Environmental Chemistry*, *88*(3), 385–394.

Reist, P.C. (1984). *Introduction to Aerosol Science*. Macmillan Publishing: New York.

Richman, J.D., Livi, K.J.T., & Geyh, A.S. (2011). A scanning transmission electron microscopy method for determining manganese composition in welding fume as a function of primary particle size. *Journal of Aerosol Science*, *42*, 408–418.

Smirnov, B.M. (2000). Cluster plasma. *Physics-Uspekhi*, *43*(5), 453–491.

Sowards, J.W., Lippold, J.C., Dickinson, D.W., & Ramirez, A.J. (2008a). Characterization procedure for the analysis of arc welding fume. *Welding Journal*, *87*(3), 76-s–83-s.

Sowards, J.W., Lippold, J.C., Dickinson, D.W., & Ramirez, A.J. (2008b). Characterization of welding fume from SMAW electrodes—Part 1. *Welding Journal* *87*(4), 106-s–112-s.

Tashiro, S., Zeniya, T., Yamamoto, K., Tanaka, M., Nakata, K., Murphy, A.B., Yamamoto, E., Yamazaki, K., & Suzuki, K. (2010). Numerical analysis of fume formation mechanism in arc welding. *Journal of Physics D: Applied Physics*, *43*, 434012 (1–12).
Vishnyakov, V.I. (2008). Homogeneous nucleation in thermal dust-electron plasmas. *Physical Review E*, *78*, 056406 (1–5).
Vishnyakov, V.I. (2012). Charging of dust in thermal collisional plasmas. *Physical Review E*, *85*, 026402 (1–6).
Vishnyakov, V.I., Kiro, S.A., & Ennan, A.A. (2013). Formation of primary particles in welding fume. *Journal of Aerosol Science*, 58, 9–16.
Voitkevich, V.G. (1995). *Welding Fumes: Formation, Properties and Biological Effects*. Abington Publishing: Cambridge.
Worobiec, A., Stefaniak, E., Kiro, S., Oprya, M., Bekshaev, A., Spolnik, Z., Potgieter-Vermaak, S.S., Ennan, A., & Van Grieken, R. (2007). Comprehensive microanalytical study of welding aerosols with X-ray and Raman based method. *X-ray Spectrometry*, *36*, 328–335.
Yu, M., Lin, J., & Chan, T. (2008). A new moment method for solving the coagulation equation for particles in Brownian motion. *Aerosol Science and Technology*, *42*, 705–713.
Zimmer, A.T., & Biswas, P. (2001). Characterization of the aerosols resulting from arc welding processes. *Journal of Aerosol Science*, *32*, 993–1008.